NIH-PA Author Manuscript
NIH-PA Author Manuscript
NIH-PA Author Manuscript

NIH Public Access
Author Manuscript
Nat Struct Mol Biol. Author manuscript; available in PMC 2012 October 09.

Published in final edited form as:
Nat Struct Mol Biol. 2008 October ; 15(10): 1076–1083. doi:10.1038/nsmb.1494.

Crystal structures of the SAM-III/S_{MK} riboswitch reveal the SAM-dependent translation inhibition mechanism

Changrui Lu[1], **Angela M Smith**[2], **Ryan T Fuchs**[2], **Fang Ding**[1], **Kanagalaghatta Rajashankar**[3], **Tina M Henkin**[2], and **Ailong Ke**[1]

[1]Department of Molecular Biology and Genetics, Cornell University, 251 Biotechnology Building, Ithaca, New York 14853, USA.

[2]Department of Microbiology and Center for RNA Biology, Ohio State University, 376 Biological Science Building, 484 West 12th Avenue, Columbus, Ohio 43210, USA.

[3]Northeastern Collaborative Access Team, Advanced Photon Source, Building 436, 9700 South Cass Avenue, Argonne, Illinois 60439, USA.

Abstract

Three distinct classes of *S*-adenosyl-L-methionine (SAM)-responsive riboswitches have been identified that regulate bacterial gene expression at the levels of transcription attenuation or translation inhibition. The S_{MK} box (SAM-III) translational riboswitch has been identified in the SAM synthetase gene in members of the Lactobacillales. Here we report the 2.2-Å crystal structure of the *Enterococcus faecalis* S_{MK} box riboswitch. The Y-shaped riboswitch organizes its conserved nucleotides around a three-way junction for SAM recognition. The Shine-Dalgarno sequence, which is sequestered by base-pairing with the anti–Shine-Dalgarno sequence in response to SAM binding, also directly participates in SAM recognition. The riboswitch makes extensive interactions with the adenosine and sulfonium moieties of SAM but does not appear to recognize the tail of the methionine moiety. We captured a structural snapshot of the S_{MK} box riboswitch sampling the near-cognate ligand *S*-adenosyl-L-homocysteine (SAH) in which SAH was found to adopt an alternative conformation and fails to make several key interactions.

Recent discoveries of *cis*-acting regulatory RNAs termed riboswitches revealed the novel ability of RNA to directly relay environmental cues to the genetic regulation machinery (for reviews, see refs. 1–3 and references therein). Bacteria use riboswitches to regulate the metabolism and transport of vitamins[4–9], nucleotides[10–15], amino acids[16–19], cofactors[5,20–24] and metal ions[25,26]. Riboswitches are especially prevalent in Gram-positive bacteria, as exemplified by *Bacillus subtilis*, where more than 4% of its genes are riboswitch regulated[27]. A handful of riboswitches were also found in eukaryotic systems, suggesting that such mechanisms may be even more widespread than currently appreciated[9,28,29].

A typical metabolite binding riboswitch consists of a ligand-sensing ‘aptamer domain’ and an ‘output domain’ that regulates gene expression, generally at the levels of transcription attenuation or translation initiation[2,4,30]. Binding of the cognate metabolite to the aptamer domain usually causes conformational changes that result in alternative base-pairing in the output domain, which in turn affects expression of the downstream open reading frames. The three classes of SAM-responsive riboswitches, including the S box (SAM-I)[20–22,31],

© 2008 Nature Publishing Group

Correspondence should be addressed to A.K. (ailong.ke@cornell.edu).

Note: Supplementary information is available on the Nature Structural & Molecular Biology website.

NIH-PA Author Manuscript

SAM-II[23] and S_{MK} box (SAM-III)[24], represent the most commonly found riboswitch families in bacterial genomes[32]. All of these riboswitches are highly selective for SAM over its natural analog SAH, which is generated from utilization of SAM as a methyl donor in enzyme-catalyzed methyltransfer reactions and differs from SAM by the absence of a methyl group and a positive charge on the sulfur atom. Crystal structures of the S box (SAM-I) and SAM-II riboswitches[33,34] revealed two completely different RNA folds that use distinct mechanisms of SAM recognition.

The S_{MK} box riboswitch (Fig. 1a) regulates the translation of SAM synthetase (*metK*) genes in lactic acid bacteria by sequestration of the Shine-Dalgarno (SD) sequence, which is essential for loading of the 30S ribosomal subunit for translation initiation[24]. Notably, the SD sequence within the S_{MK} box family (GGGGG) differs from the consensus SD sequence (GGAGG) at the central position (Fig. 1a,b). The three Gs at the 3′ portion of the SD sequence, in conjunction with the following two nucleotides, base pair with the anti–Shine-Dalgarno (ASD) sequence in the presence of SAM[24], which hinders the binding of 30S ribosomal subunits to the mRNA[35]. Mutational studies demonstrated that the S_{MK} box riboswitch differs from most metabolite binding riboswitches in that the SD-ASD pairing is required for SAM binding, indicating that the output domain (the SD-ASD pairing) is an intrinsic part of the ligand binding domain[24]. Similarly to other SAM riboswitches, the S_{MK} box riboswitch shows at least 100-fold preference for SAM over SAH (refs. 24,35 and this study).

To elucidate the SAM-induced translation-inhibition mechanism in the S_{MK} box riboswitch, we determined crystal structures of the *E. faecalis* S_{MK} box riboswitch, including its SD sequence, in the presence of SAM, selenium-derivitized SAM (Se-SAM) or SAH. The RNA was found to organize into a Y-shaped molecule, with SAM intercalated into the three-way helical junction (Fig. 1c). In agreement with previous genetic and enzymatic probing analyses[24,35], the SD sequence contributes to both binding-site formation and specific SAM recognition. The near-cognate ligand SAH can make only weak and nonspecific interactions with the riboswitch.

NIH-PA Author Manuscript

RESULTS

Structure determination

We determined the crystal structure of the *E. faecalis* S_{MK} box riboswitch[24] to elucidate the SAM-dependent translation-inhibition mechanism. The optimized version of the S_{MK} box riboswitch (Fig. 1b and Supplementary Methods online), designated S_{MK}6, allowed structure determination at 2.2 Å and showed SAM binding activity similar to that of the full-length wild-type construct (Fig. 2a,b). The apparent K_d values for SAM determined by size-exclusion filtration were estimated to be 0.85 μM for the full-length transcript (corresponding to positions 15–118 relative to the predicted *E. faecalis metK* transcription start site)[24] and 0.57 μM for the 53-nucleotide (nt) crystallization construct (Fig. 2b). The K_d value for the full-length S_{MK} transcript was further confirmed by fluorescence-quenching assays (Supplementary Fig. 1 and Supplementary Results online). In a competition assay, the S_{MK} box riboswitch shows at least 100-fold preference for SAM over its near-cognate ligand SAH[24] (Fig. 2b).

NIH-PA Author Manuscript

Overall structure of the S_{MK} box riboswitch

The 53-nt S_{MK} box riboswitch RNA folds into an inverted Y-shaped molecule, where helices P1 (SD-ASD helix) and P4 (linker helix) constitute the two short arms, and P3 (top helix) stacks on top of P2 (middle helix) to give rise to the long arm (Fig. 1c). Most of the secondary-structure features match the predictions from the phylogenetic analysis and

NIH-PA Author Manuscript

RNase T1, V1, A and H probing experiments[24], including the SAM-dependent formation of the SD-ASD helix and the protection of nucleotides including U69, U70, C75 and G88, although the P4 linker helix was not previously assigned. The quintuple-G SD sequence spans the SD-ASD (P1) and linker (P4) helices (Fig. 1b), contributing to the overall folding of the RNA and the SAM binding site. Among the 23 residues in the S_{MK} box riboswitch that are 100% conserved (Fig. 1a), 10 participate in the formation of a pocket inside the three-way junction, where the adenosine moiety of SAM intercalates to allow continuous base stacking from P1 to P2. A lid-like structure formed as a result of a double-strand reversal in the J3/2 bulge partially encloses the SAM binding site and further stabilizes the three-way junction through base-triple interactions that enlarge the major groove of P2. A total of 15 divalent metal ions were identified bound to the S_{MK} RNA to shield the unfavorable electrostatic interactions between sugar phosphate backbones as the result of tertiary RNA folding (Supplementary Fig. 2 and Supplementary Table 1 online).

The P4 linker helix was further probed by poly(A) scanning mutations. Replacement of the 11-nt hypervariable *E. faecalis* linker region with a poly$(A)_6$ sequence did not affect SAM binding activity; disrupting the linker helix by further mutating G88 and G89 to adenosine residues, however, dramatically reduced SAM binding (Fig. 2a), consistent with the participation of these residues in the P4 linker helix. Additional point mutations were generated to confirm the formation of the G88-C76 base pair (Fig. 2a). Introduction of a C76U wobble mutation in the *E. faecalis* S_{MK} box, which occurs naturally in some S_{MK} box family members when a third 77–87 base pair is maintained[24], resulted in retention of 59% of the SAM binding activity. By contrast, the G88A mismatch mutation that would severely destabilize the linker helix resulted in a 75-fold reduction in SAM binding activity. Combination of the C76U and G88A mutations, which replaces the G-C pair with a weaker A-U pair, restored the binding to 32% of the wild-type level, consistent with sequence-alignment results that suggest that an additional base pair is needed in this context to maintain the stability of the linker helix[24].

Binding-pocket formation

The floor of the SAM binding pocket (Fig. 3a) is defined by a crucial base-triple interaction (A73•G90-C25), where N1 of A73 approaches from the minor groove side to accept a hydrogen bond from N2 of G90 (Fig. 3b). This base triple serves two purposes: first, it ties J2/4 to the P1 SD-ASD helix in conjunction with another interaction between the N1 of A74 and the 2′-hydroxyl of G90; furthermore, it orients the N6 amine of A73 for SAM recognition. Base-pairing at C25-G90 is crucial, as a C25•A90 mismatch (G90A mutation) reduced the SAM binding activity to 1.3% of the wild type, whereas a U25-G90 wobble pair (C25U mutation) showed 63% of the SAM binding activity (Fig. 2a). The importance of the A73•G90-C25 base triple is underlined by the strong, deleterious effect of the C25U G90A double mutation, which converts the SD element from the quintuple-G sequence found in all S_{MK} box elements to the more commonly found GGAGG sequence, while maintaining the SD-ASD pairing. The loss of SAM binding activity in this mutant is apparently due to the loss of N2 when G90 is converted to A, which disrupts the A73•G90 side of the base-triple interaction. Thus, the structural and mutational data collectively explain the absolute conservation of an unusual SD sequence in all S_{MK} box riboswitch RNAs.

The ceiling of the SAM binding site is formed from two layers of nonstandard base pairs, both of which involve bases from the J3/2 trinucleotide bulge, which are highly conserved among the *E. faecalis* subfamily of the S_{MK} box RNAs[24]. A sheared U72•A64 pair sits immediately on top of the SAM intercalation base plane, which exposes the O4 of U72 for SAM recognition. Further above is the A27•G71•G66 base triple, where G71 mediates extensive hydrogen bond contacts to the Hoogsteen face of both A27 and G66, weaving P2 together with J3/2 (Fig. 3c). U65 in the J3/2 bulge mediates a U-turn motif and extends

NIH-PA Author Manuscript

NIH-PA Author Manuscript

NIH-PA Author Manuscript

toward the opening of the SAM binding pocket; this residue was shown to be more prone to RNase T1 digestion in the presence of SAM[24], consistent with the proposal that SAM binding reorients this residue. The backbone of the bulge resembles a ‘lid’ that secludes SAM inside the three-way junction and contributes to the overall electronegative environment inside the pocket, which may help to attract the SAM molecule. The importance of the J3/2 lid structure is indicated by the U65C and U65 deletion mutations, which cause a 5-fold and 20-fold decrease in SAM binding activity, respectively (Fig. 2a).

SAM recognition

The universally conserved G26 is left unpaired inside the cavity of the three-way junction. SAM intercalates its adenosine moiety between the P1 and P2 helices from the major groove side, stabilizing the three-way junction through π-stacking interactions (Fig. 3d). The adenosine moiety of SAM adopts an energetically unfavorable *syn*-conformation and presents its Watson-Crick face to form three minor groove contacts (N1-amino, amino-N3 and amino-2′-OH) with the unpaired G26. Even a minor perturbation of the G26-SAM interaction, such as occurs in the G26A mutant, in which the N1-amino hydrogen bond is disrupted, reduces SAM binding by five-fold (Fig. 2a). The N7 at the Hoogsteen face accepts a hydrogen bond from the N6 amine of the tilted A73 (Fig. 3d). Disruption of this hydrogen bond by the A73G mutation caused an 80-fold reduction in SAM binding activity (Fig. 2a), although we cannot completely separate this effect from the disruption of the A73•G90-C25 base triple. The ribose moiety of SAM adopts a 2′-endo conformation to avoid steric clashes with the base plane of G89 in the SD sequence[36]. The 2′- and 3′-hydroxyl groups of SAM are recognized by hydrogen bonds to the N7 (π-hydrogen bond) and 2′-hydroxyl of G89, respectively (Fig. 3e). The 2′-hydroxyl of SAM donates an additional water-mediated hydrogen bond to the N6 of A74.

The positive charge on the sulfonium ion of SAM is recognized through favorable electrostatic interactions with the O4 carbonyl of U72 and the 2′-hydroxyl of G71 (Fig. 3f). The positive charge is further stabilized through intramolecular electrostatic interactions with the O4′ on the ribose and N3 on the base of SAM (Fig. 3d). Consistent with the structural observations, the U72C mutation, which places a partially positive N4 amine toward the sulfonium, decreases the SAM binding activity by 70-fold (Fig. 2a). A similar charge-stabilization scheme involving contacts between the sulfonium ion of SAM and O4 of uracil is used by the other two classes of SAM binding riboswitches to selectively bind the SAM molecule[33,34]. The neutral, hydrophobic sulfide in SAH is not expected to make these electrostatic interactions with the RNA.

In contrast to the well-defined adenosine moiety, no electron density was observed for functional groups beyond the sulfonium ion in SAM (Fig. 3d). This is a strong indication that the methionine tail (including the main chain and most of the side chain atoms beyond the sulfur) is not specifically recognized by the S_{MK} box riboswitch, which is in sharp contrast to the extensive recognition of the methionine tail observed in the structures of the S box and SAM-II riboswitches[33,34]. Lack of recognition toward the methionine tail is further supported by binding studies with SAM analogs, where SAM analogs lacking the methionine main chain atoms bind the S_{MK} box riboswitch with affinities similar to that of SAM (A.M.S., F.J. Grundy and T.M.H., unpublished data). The methyl group on the sulfonium ion is not specified by the S_{MK} box riboswitch (Fig. 3d) because replacing it with an ethyl group does not impair ligand-RNA interactions (A.M.S., F.J. Grundy and T.M.H., unpublished data). The modeled methionine conformation illustrated in Figure 3 complies with all spatial constraints derived from the structural and SAM-analog studies.

NIH-PA Author Manuscript NIH-PA Author Manuscript NIH-PA Author Manuscript

Regulation of *E. faecalis metK-lacZ* fusions *in vivo*

The *E. faecalis metK* S_{MK} box was previously shown to confer translational regulation of a *lacZ* reporter gene in which the translation-initiation region is replaced by that of the *metK* gene[24]. Integration of the fusion construct into the *B. subtilis* chromosome results in high expression when cells are grown under conditions where intracellular SAM pools are low and a five-fold reduction in expression when cells are grown in the presence of high methionine concentrations, conditions that result in high SAM pools[37].

The S_{MK} box riboswitch structure supports the model that SAM-dependent SD-ASD helix formation is responsible for translational inhibition. To verify this hypothesis, we evaluated the functional consequences of three sets of mutations that perturb the stability of the SD-ASD helix. As previously reported[24], a C24G mutation in the ASD region, predicted to disrupt the SD-ASD interaction, causes loss of repression *in vivo* (Table 1) and loss of SAM binding (Fig. 2a). A C24U mutation had a similar effect (Table 1), although expression was significantly higher and a small response to SAM was retained, presumably because of the maintenance of a U24-G91 wobble pairing. A C24U G91A double mutation, which restores pairing at this position, restored SAM binding (Fig. 2a) and resulted in low expression but only partial restoration of repression by SAM (Table 1). The low expression is likely to be due to disruption of the SD by the G91A mutation, which causes reduced affinity for 30S ribosomal subunits and therefore obscures the regulatory response *in vivo*. A similar pattern was observed with the U22G and A93C mutations (Table 1), which affect the ASD and SD sequences, respectively, and cause loss of SAM binding *in vitro*[35]. The U22G A93C double mutant restores the pairing at this position and restores SAM binding[35]. This mutant also showed SAM-dependent repression *in vivo*, although expression was reduced relative to that of the wild-type construct (Table 1). This reduction in expression may be due to an enhanced SD-ASD interaction from replacing an A-U pair with a G-C pair.

As described above, G90 in the SD sequence has a pivotal role in the S_{MK} box riboswitch, as it organizes the SAM binding pocket through A73•G90-C25 base-triple formation and stacks directly underneath the SAM molecule. The C25U substitution creates a wobble pair with G90. This mutant showed partial repression by high SAM concentrations *in vivo* (Table 1), consistent with a modest reduction of SAM binding *in vitro* (Fig. 2a). The C25U G90A double mutant is predicted to restore Watson-Crick pairing at this position but not the crucial base-triple interaction with A73. This variant showed complete loss of repression *in vivo*, despite maintaining a canonical SD sequence (Table 1), in accordance with the loss of SAM binding *in vitro* (Fig. 2a). These data confirm the importance of G90 for SAM binding and SAM-dependent regulation.

Se-SAM–bound S_{MK} box structure confirms sulfonium position

To confirm the position of the sulfur atom in the SAM molecule, we further determined the structure of the S_{MK} box riboswitch soaked in freshly prepared Se-SAM (where the sulfur atom is substituted with selenium, a heavier chalcogen analog[38]). The conformations of the RNA and the Se-SAM molecule are essentially identical to that in the SAM-bound structure, with an r.m.s. deviation of 0.3 Å for all-phosphorous-atom alignment. The same set of contacts specifies Se-SAM in the ligand binding site, and the selenomethionine moiety remains unstructured beyond the onium selenium (Fig. 4a). The location of the selenium atom, which essentially overlaps with the sulfur atom in the omit map, is unambiguously identified by an 8σ anomalous difference signal collected at the absorption edge of selenium (Fig. 4a). The distances of the electrostatic interactions between the RNA and the onium selenium are on average ~0.3 Å longer than seen in the SAM-bound structure, reflecting the increased van der Waals radius. Observations from the Se-SAM–bound riboswitch structure

NIH-PA Author Manuscript

NIH-PA Author Manuscript

NIH-PA Author Manuscript

confirm our assignment of the sulfonium position in SAM and strengthen our conclusion that the methionine tail of SAM is not specified by the S_{MK} box riboswitch.

SAH makes a minimum set of contacts to the S_{MK} box riboswitch

To investigate how the S_{MK} box riboswitch would respond in the presence of natural near-cognate ligands such as SAH, we determined the S_{MK} box RNA structure in the presence of SAH at a saturating concentration of 2 mM, about 67- to 2,000-fold higher than the intracellular concentration of SAH (0.5–30 μM[39]). The resulting structure revealed that SAH can displace SAM at saturating concentration. The binding pocket and overall structure of the S_{MK} box riboswitch remains unchanged, presumably owing to strong crystal lattice contacts to the P1 and P4 helices. The resulting structure is thus a snapshot of the functional S_{MK} box riboswitch sampling a near-cognate ligand before rejecting it. In the 2.9-Å resolution structure, SAH adopts a conformation very different from SAM in the binding pocket (Fig. 4b). The ribose moiety of SAH rotates 180°, such that the adenosine moiety now adopts an *anti*-conformation. 2′- and 3′-hydroxyls in SAH make an alternative set of interactions with the phosphoryl oxygens of G90. More importantly, weak electron-density features revealed that the uncharged sulfide in SAH rotates 180° from U72 to the vicinity of G71. As a result, the intramolecular contacts that stabilize the sulfonium ion conformation in SAM and the key electrostatic interactions between the sulfur atom and the RNA are all lost when SAH is in place. It therefore seems that the positive charge on the sulfur atom is crucial in presenting the SAM molecule in the correct conformation for strong ligand-RNA interactions, analogous to the 'lock-and-key' mechanism found in many enzyme-substrate complexes. The structural observations are consistent with *in vitro* assays showing that the S_{MK} box riboswitch has much higher affinity for SAM over SAH[24,35], with at least a 100-fold preference for SAM.

DISCUSSION

With the completion of the structure of the S_{MK} box riboswitch, a family portrait of the three known classes of SAM binding riboswitches is now available[33,34]. These riboswitches adopt completely different RNA folds and have probably emerged independently during evolution. They nevertheless converged at the functional level to preferentially recognize SAM, an important metabolite inside the cell, and regulate gene expression in response to the ligand binding event. We conclude from structural comparisons that, although creative ways are used to accommodate the binding of SAM, a conserved mechanism is used by all three classes of SAM riboswitches to distinguish SAM from SAH, which is the biologically relevant SAM analog.

Riboswitches sense both chemical and conformational distinctions in SAM

SAM adopts drastically different conformations among the three classes of SAM riboswitches (Supplementary Fig. 3a online). The *Thermoanaerobacter tengcongensis* and *B. subtilis yitJ* S box (SAM-I) riboswitches completely engulf SAM in a pocket between two helical stacks (ref. 33 and C.L. *et al.*, unpublished data). The SAM-II riboswitch adopts a classic H-type pseudoknot and encloses SAM inside an RNA triple helix[34]. The S_{MK} box riboswitch allows the intercalation of SAM into a tight pocket in a three-way junction. In each case, SAM mediates important tertiary interactions to stabilize the ligand-bound conformation of the riboswitch. The adenine base is involved in base stacking and base-triple interactions in all three riboswitches. The positively charged sulfonium moiety is invariably recognized through favorable electrostatic interactions, usually with one or two O4 carbonyl oxygen atoms from uracil residues. This recognition forms the basis for preferential binding of SAM over SAH. The methyl group on the sulfonium moiety is not directly contacted by any of the three riboswitches. Rather, it points toward the solvent

NIH-PA Author Manuscript NIH-PA Author Manuscript NIH-PA Author Manuscript

region and is recognized collectively with the sulfonium ion, a mechanism perhaps evolved to prevent self inactivation by spontaneous methylation of the RNA by SAM. Recognition of the methionine tail, however, occurs differently in the three riboswitches. The tail is extensively contacted by the S box riboswitch[33], less so by the SAM-II riboswitch[34] and completely ignored by the S_{MK} box riboswitch. Previous structural studies seem to suggest that riboswitches are more likely to be identified through bioinformatics rather than SELEX approaches because in each structure, the metabolite is completely encapsulated by the RNA. The ability of the biologically active S_{MK} box riboswitch to recognize SAM by specifying only half of the molecule and without engulfing SAM completely suggests that additional classes of SAM riboswitches can potentially be identified by SELEX approaches using a SAM molecule immobilized at the methionine tail as the bait.

In addition to chemical differences between SAM and SAH, SAM also adopts a distinct conformation that is energetically unfavorable for SAH and other noncognate SAM analogs. Alignment of the conformations of SAM within the three riboswitch structures along the ribose region clearly revealed that, although the conformation of the adenine base (*syn*- or *anti*-) and the methionine tail (crouched or extended) varies dramatically among the three riboswitch structures, the sulfonium ion makes an invariable, strong 3-Å electrostatic contact to the O4′ of the SAM ribose (Supplementary Fig. 3a,b). This *gauche*-conformation (Supplementary Fig. 3b) about the C4′–C5′ bond has been shown by NMR measurement to be the predominant (93%) SAM conformation in solution[36]. The same study showed that SAH, on the other hand, favors the *anti*-conformation[36], presumably because of its inability to maintain the intramolecular electrostatic interaction. Indeed, in our survey of 30 randomly chosen SAH-bound protein structures, 87% of the SAH molecules adopted the *anti*-conformation (Supplementary Fig. 3b). Thus, by simultaneously contacting both the ribose and the sulfonium moieties of SAM, all three riboswitches effectively select for a SAM conformation that is unfavorable for SAH. Consistent with this observation, our structural analysis of the SAH-bound S_{MK} box riboswitch revealed that, although SAH could bind to the crystalline-trapped S_{MK} box riboswitch at a nonphysiological high concentration, the sulfide moiety in the riboswitch-bound form of SAH swings 180° away from the sulfonium binding site, severely weakening the ligand-RNA interactions to a level indistinguishable from the binding of other adenosine-containing metabolites such as ATP. Thus, it seems that both chemical and conformational differences at the sugar-sulfur linkage are explored by SAM binding riboswitches to distinguish between cognate and near-cognate ligands. The recent discovery of a new class of SAH binding riboswitches upstream of bacterial genes involved in SAM recycling[40] demonstrates that RNA is capable of forming a selective binding site that favors either SAM or SAH.

A simple SAM-dependent translation-inhibition mechanism

A typical riboswitch is conceptually modular, consisting of a ligand-sensing aptamer domain and a separate output domain whose structure is influenced by the ligand binding event at the aptamer domain. A much simpler mechanism for translational regulation is found in the S_{MK} box and SAM-II riboswitches, where the SD sequence is an integral part of the SAM binding aptamer domain, allowing ligand sensing and translational inhibition through SD-sequence sequestration to take place in a single step. An important feature in the S_{MK} box riboswitch is the direct involvement of the SD sequence in SAM recognition. Although strong crystal packing interactions prevent observation of large ligand-induced conformational changes in crystal structures, mutagenesis and enzymatic probing assays[24,35] clearly revealed global conformational changes in the presence of physiologically relevant concentrations of SAM but not SAH. These SAM-dependent changes are especially evident in the formation of the linker and SD-ASD helices that sequester the ribosome binding site. Conversely, the ability to form the linker and SD-ASD helices is a prerequisite for SAM

NIH-PA Author Manuscript

NIH-PA Author Manuscript

NIH-PA Author Manuscript

binding[24]. The combined structural and biochemical data suggest that SAM shifts the conformational equilibrium toward the ligand-bound state seen in the crystal structure, where the SD sequence required for binding of the 30S ribosomal subunit is sequestered. Consistent with this mechanism, ribosome toeprinting analysis showed that the correct positioning of the 30S ribosomal subunit on the S_{MK} box mRNA is reduced in the presence of SAM but not SAH[35]. Direct involvement of the SD sequence in the formation of the aptamer domain is also observed in the SAM-II riboswitch structure[34], although the exact location of the SD sequence is less well defined.

In summary, our combined structural and mutagenesis data on the S_{MK} box riboswitch clearly demonstrate its mechanism for translational inhibition through sequestration of the SD sequence, and the interplay between SD-ASD pairing and SAM binding activity. The S_{MK} box riboswitch is unique among riboswitch RNAs studied to date in that the same residues of the RNA that are involved in gene regulation (the SD sequence) are directly involved in specific recognition of the SAM ligand.

METHODS

RNA crystallization and structure determination

Design of the crystallization construct is described in the Supplementary Methods. RNA was prepared as described[41]. Se-SAM was a gift from S. Booker (Pennsylvania State University). Its synthesis has been described previously[38]. SAM and SAH were purchased from Sigma, dissolved in water and DMSO, respectively, as 100 mM stock solutions (pH < 7) and stored at −80 °C until immediately before use.

To ensure conformational homogeneity, the S_{MK} box RNA was heat-refolded as described[24,35]. The high-resolution $S_{MK}6$ crystals grew as extremely slim needle crystals of $15 \times 15\ \mu m^2$ in cross-section from a solution containing 40 mM sodium cacodylate, pH 7.0, 80 mM strontium chloride, 15% (w/v) 2-methylpentane-2,4-diol (MPD) and 2 mM spermine-HCl. The MPD content was raised stepwise to 25% (w/v) before the crystals were flash-frozen in liquid nitrogen. Diffraction data were collected using the microcrystallography setup at beamlines Advanced Photon Source (APS) 24-ID-E and MACCHESS F1 and processed using HKL2000[42]. The detailed phasing and refinement procedure is described in the Supplementary Methods. The initial model was built using COOT[43] from experimental phases calculated from SHELXD[44] and refined using Refmac5[45] and CNS[46,47]. The final model includes all nucleotides and a total of 15 strontium ions (Supplementary Table 1) and 69 water molecules. The methionine tail of SAM and the pyrimidine ring of U65 are the only portion of the model without corresponding electron densities. Final R_{work} and R_{free} factors were 22.1% and 22.7%, respectively (Table 2). Se-SAM and SAH bound structures were determined by molecular replacement using PHASER[48] and refined using Refmac5 (ref. 45) and CNS[46,47] (Table 2 and Supplementary Methods).

In vitro SAM binding assays

We carried out SAM binding assays as previously described[24,35] with minor modifications. DNA templates corresponding to positions 15–118 (relative to the predicted transcription start site) of the *E. faecalis metK* leader were constructed by ligating overlapping pairs of complementary oligonucleotides, including a T7 RNA polymerase promoter sequence, as previously described[49,50]. Ligated products were amplified by PCR and RNAs were synthesized by T7 RNA polymerase transcription using an AmpliScribe T7 High Yield Transcription Kit (Epicentre Biotechnologies). RNAs (3 μM) in 1× transcription buffer[51] were heated to 65 °C for 5 min and slow-cooled to 40 °C, followed by addition of

NIH-PA Author Manuscript NIH-PA Author Manuscript NIH-PA Author Manuscript

radiolabeled SAM (3 μM [methyl-^{3}H]-SAM, 15 Ci mmol^{-1}; GE Healthcare) in a total reaction volume of 40 μl. Binding reactions were incubated at room temperature (20–25 °C) for 15 min followed by passage through a Nanosep 10K Omega filter (Pall Life Sciences) by centrifugation at 14,000*g* for 2.5 min. Filters were washed four times with 40 μl 1× transcription buffer to remove unbound SAM, and material retained by the filter was collected, mixed with Packard BioScience Ultima Gold scintillation fluid and counted in a Packard Tri-Carb 2100TR liquid scintillation counter. No SAM was retained by the filter in the absence of RNA; hence, the background for nonspecific binding is negligible. All binding assays were carried out in triplicate and the s.d. are shown in Figure 2.

Apparent K_d determination

The apparent equilibrium dissociation constants (K_d values) for the wild-type 15–118 *metK* leader sequence and the 53-nucleotide crystallization construct were determined using a modified SAM binding assay[37]. Briefly, T7 RNA polymerase transcribed RNA (1 μM) in 1× transcription buffer[51] was refolded as described above and incubated with [^{3}H]-SAM ranging in concentration from 0.02 μM to 10 μM. Binding reactions were loaded onto Nanosep 3K Omega filters (Pall Life Sciences) and centrifuged briefly at 14,000*g* to avoid large volume changes. The concentration of the RNA-[^{3}H]-SAM complex retained by the filter and the unbound SAM present in the flow through were determined by scintillation counting of known volumes, and nonlinear regression analyses were performed using Kaleida-Graph Version 3.51 (Synergy Software). Apparent K_d values represent the averages of at least two independent experiments for each construct with a margin of error ≤ 5%.

In vivo lacZ reporter gene assay of S_{MK} box fusions

We carried out *in vivo lacZ* reporter gene assays as described previously[24,35]. *Enterococcus faecalis metK* leader region constructs, which included the first 15 nt of the coding region, were positioned downstream of the highly expressed *B. subtilis glyQS* promoter. The resulting DNA fragment was inserted into a *lacZ* fusion vector (pFG328)[52] to generate an in-frame *metK*-*lacZ* translational fusion in which the first five codons of *metK* were fused to codon 18 of *lacZ*. The constructs were introduced into the chromosome of *B. subtilis* strain BR151 (*metB10 lys-3 trpC2*) by integration into an SPβ prophage. *Bacillus subtilis* strains containing the *lacZ* fusions were grown at 37 °C in Spizizen minimal medium[53] containing methionine (50 μg ml^{-1}) until early exponential growth. The cells were harvested by centrifugation at 8,000*g* and resuspended in Spizizen medium either with or without methionine, and samples were collected at 1-h intervals and assayed for β-galactosidase activity after toluene permeabilization of the cells[54]. All assays were carried out in triplicate and the s.d. are shown in Table 1.

Accession codes

Protein Data Bank: Structure factors and coordinates for the SAM, SAH and Se-SAM bound S_{MK} box riboswitch have been deposited in the Protein Data Bank with accession numbers 3E5C, 3E5E and 3E5F, respectively.

Supplementary Material

Refer to Web version on PubMed Central for supplementary material.

Acknowledgments

We thank S. Booker at Pennsylvania State University for the gift of the Se-SAM; Q. Hao, R. Gillian and other beam line staff at MACCHESS and APS ID24 for assistance in data collection; F. Grundy for assistance in SAM binding assay design; and J. Doudna for helpful discussions and comments on the manuscript. Work in the Henkin laboratory was supported by a Public Health Service grant (GM63615) from the US National Institutes of Health

NIH-PA Author Manuscript

(NIH). This work is based upon research conducted at the Northeastern Collaborative Access Team beamlines of the Advanced Photon Source, which is supported by National Cancer Institute (NCI) award RR-15301 and DOE contract No. DE-AC02-06CH11357, and at the Cornell High Energy Synchrotron Source (CHESS), which is supported by the National Science Foundation award DMR 0225180 and the NCI award RR-01646.

References

1. Tucker BJ, Breaker RR. Riboswitches as versatile gene control elements. Curr. Opin. Struct. Biol. 2005; 15:342–348. [PubMed: 15919195]
2. Grundy FJ, Henkin TM. From ribosome to riboswitch: control of gene expression in bacteria by RNA structural rearrangements. Crit. Rev. Biochem. Mol. Biol. 2006; 41:329–338. [PubMed: 17092822]
3. Vitreschak AG, Rodionov DA, Mironov AA, Gelfand MS. Riboswitches: the oldest mechanism for the regulation of gene expression? Trends Genet. 2004; 20:44–50. [PubMed: 14698618]
4. Winkler W, Nahvi A, Breaker RR. Thiamine derivatives bind messenger RNAs directly to regulate bacterial gene expression. Nature. 2002; 419:952–956. [PubMed: 12410317]
5. Wickiser JK, Winkler WC, Breaker RR, Crothers DM. The speed of RNA transcription and metabolite binding kinetics operate an FMN riboswitch. Mol. Cell. 2005; 18:49–60. [PubMed: 15808508]
6. Serganov A, Polonskaia A, Phan AT, Breaker RR, Patel DJ. Structural basis for gene regulation by a thiamine pyrophosphate-sensing riboswitch. Nature. 2006; 441:1167–1171. [PubMed: 16728979]
7. Winkler WC, Cohen-Chalamish S, Breaker RR. An mRNA structure that controls gene expression by binding FMN. Proc. Natl. Acad. Sci. USA. 2002; 99:15908–15913. [PubMed: 12456892]
8. Sudarsan N, Cohen-Chalamish S, Nakamura S, Emilsson GM, Breaker RR. Thiamine pyrophosphate riboswitches are targets for the antimicrobial compound pyrithiamine. Chem. Biol. 2005; 12:1325–1335. [PubMed: 16356850]
9. Thore S, Leibundgut M, Ban N. Structure of the eukaryotic thiamine pyrophosphate riboswitch with its regulatory ligand. Science. 2006; 312:1208–1211. [PubMed: 16675665]
10. Christiansen LC, Schou S, Nygaard P, Saxild HH. Xanthine metabolism in *Bacillus subtilis*: characterization of the *xpt-pbuX* operon and evidence for purine- and nitrogen-controlled expression of genes involved in xanthine salvage and catabolism. J. Bacteriol. 1997; 179:2540–2550. [PubMed: 9098051]
11. Mandal M, Breaker RR. Adenine riboswitches and gene activation by disruption of a transcription terminator. Nat. Struct. Mol. Biol. 2004; 11:29–35. [PubMed: 14718920]
12. Mandal M, Boese B, Barrick JE, Winkler WC, Breaker RR. Riboswitches control fundamental biochemical pathways in *Bacillus subtilis* and other bacteria. Cell. 2003; 113:577–586. [PubMed: 12787499]
13. Roth A, et al. A riboswitch selective for the queuosine precursor preQ1 contains an unusually small aptamer domain. Nat. Struct. Mol. Biol. 2007; 14:308–317. [PubMed: 17384645]
14. Kim JN, Roth A, Breaker RR. Guanine riboswitch variants from *Mesoplasma florum* selectively recognize 2′-deoxyguanosine. Proc. Natl. Acad. Sci. USA. 2007; 104:16092–16097. [PubMed: 17911257]
15. Meyer MM, Roth A, Chervin SM, Garcia GA, Breaker RR. Confirmation of a second natural preQ1 aptamer class in *Streptococcaceae* bacteria. RNA. 2008; 14:685–695. [PubMed: 18305186]
16. Mandal M, et al. A glycine-dependent riboswitch that uses cooperative binding to control gene expression. Science. 2004; 306:275–279. [PubMed: 15472076]
17. Rodionov DA, Vitreschak AG, Mironov AA, Gelfand MS. Regulation of lysine biosynthesis and transport genes in bacteria: yet another RNA riboswitch? Nucleic Acids Res. 2003; 31:6748–6757. [PubMed: 14627808]
18. Sudarsan N, Wickiser JK, Nakamura S, Ebert MS, Breaker RR. An mRNA structure in bacteria that controls gene expression by binding lysine. Genes Dev. 2003; 17:2688–2697. [PubMed: 14597663]
19. Grundy FJ, Lehman SC, Henkin TM. The L box regulon: lysine sensing by leader RNAs of bacterial lysine biosynthesis genes. Proc. Natl. Acad. Sci. USA. 2003; 100:12057–12062. [PubMed: 14523230]

NIH-PA Author Manuscript

20. Winkler WC, Nahvi A, Sudarsan N, Barrick JE, Breaker RR. An mRNA structure that controls gene expression by binding *S*-adenosylmethionine. Nat. Struct. Biol. 2003; 10:701–707. [PubMed: 12910260]
21. McDaniel BA, Grundy FJ, Artsimovitch I, Henkin TM. Transcription termination control of the S box system: direct measurement of *S*-adenosylmethionine by the leader RNA. Proc. Natl. Acad. Sci. USA. 2003; 100:3083–3088. [PubMed: 12626738]
22. Epshtein V, Mironov AS, Nudler E. The riboswitch-mediated control of sulfur metabolism in bacteria. Proc. Natl. Acad. Sci. USA. 2003; 100:5052–5056. [PubMed: 12702767]
23. Corbino KA, et al. Evidence for a second class of *S*-adenosylmethionine riboswitches and other regulatory RNA motifs in α-proteobacteria. Genome Biol. 2005; 6:R70. [PubMed: 16086852]
24. Fuchs RT, Grundy FJ, Henkin TM. The S_{MK} box is a new SAM-binding RNA for translational regulation of SAM synthetase. Nat. Struct. Mol. Biol. 2006; 13:226–233. [PubMed: 16491091]
25. Groisman EA, Cromie MJ, Shi Y, Latifi TA. Mg^{2+}-responding RNA that controls the expression of a Mg^{2+} transporter. Cold Spring Harb. Symp. Quant. Biol. 2006; 71:251–258. [PubMed: 17381304]
26. Coppins RL, Hall KB, Groisman EA. The intricate world of riboswitches. Curr. Opin. Microbiol. 2007; 10:176–181. [PubMed: 17383225]
27. Winkler WC. Metabolic monitoring by bacterial mRNAs. Arch. Microbiol. 2005; 183:151–159. [PubMed: 15750802]
28. Sudarsan N, Barrick JE, Breaker RR. Metabolite-binding RNA domains are present in the genes of eukaryotes. RNA. 2003; 9:644–647. [PubMed: 12756322]
29. Cheah MT, Wachter A, Sudarsan N, Breaker RR. Control of alternative RNA splicing and gene expression by eukaryotic riboswitches. Nature. 2007; 447:497–500. [PubMed: 17468745]
30. Henkin TM, Yanofsky C. Regulation by transcription attenuation in bacteria: how RNA provides instructions for transcription termination/antitermination decisions. Bioessays. 2002; 24:700–707. [PubMed: 12210530]
31. Grundy FJ, Henkin TM. The S box regulon: a new global transcription termination control system for methionine and cysteine biosynthesis genes in Gram-positive bacteria. Mol. Microbiol. 1998; 30:737–749. [PubMed: 10094622]
32. Barrick JE, Breaker RR. The distributions, mechanisms, and structures of metabolite-binding riboswitches. Genome Biol. 2007; 8:R239. [PubMed: 17997835]
33. Montange RK, Batey RT. Structure of the *S*-adenosylmethionine riboswitch regulatory mRNA element. Nature. 2006; 441:1172–1175. [PubMed: 16810258]
34. Gilbert SD, Rambo RP, Van Tyne D, Batey RT. Structure of the SAM-II riboswitch bound to *S*-adenosylmethionine. Nat. Struct. Mol. Biol. 2008; 15:177–182. [PubMed: 18204466]
35. Fuchs RT, Grundy FJ, Henkin TM. *S*-adenosylmethionine directly inhibits binding of 30S ribosomal subunits to the S_{MK} box translational riboswitch RNA. Proc. Natl. Acad. Sci. USA. 2007; 104:4876–4880. [PubMed: 17360376]
36. Stolowitz ML, Minch MJ. *S*-adenosyl-L-methionine and 5′-adenosyl-L-homocysteine, an NMR Study. J. Am. Chem. Soc. 1981; 103:6015–6019.
37. Tomsic J, McDaniel BA, Grundy FJ, Henkin TM. Natural variability in SAM-dependent riboswitches: S box elements in *Bacillus subtilis* exhibit differential sensitivity to SAM *in vivo* and *in vitro*. J. Bacteriol. 2007; 190:823–833. [PubMed: 18039762]
38. Iwig DF, Booker SJ. Insight into the polar reactivity of the onium chalcogen analogues of *S*-adenosyl-L-methionine. Biochemistry. 2004; 43:13496–13509. [PubMed: 15491157]
39. Ueland PM. Pharmacological and biochemical aspects of *S*-adenosylhomocysteine and *S*-adenosylhomocysteine hydrolase. Pharmacol. Rev. 1982; 34:223–253. [PubMed: 6760211]
40. Wang JX, Lee ER, Morales DR, Lim J, Breaker RR. Riboswitches that sense *S*-adenosylhomocysteine and activate genes involved in coenzyme recycling. Mol. Cell. 2008; 29:691–702. [PubMed: 18374645]
41. Ke A, Doudna JA. Crystallization of RNA and RNA-protein complexes. Methods. 2004; 34:408–414. [PubMed: 15325657]

NIH-PA Author Manuscript NIH-PA Author Manuscript NIH-PA Author Manuscript

42. Otwinowski Z, Minor W. Processing of X-ray diffraction data collected in oscillation mode. Methods Enzymol. 1997; 276:307–326.
43. Emsley P, Cowtan K. Coot: model-building tools for molecular graphics. Acta Crystallogr. D Biol. Crystallogr. 2004; 60:2126–2132. [PubMed: 15572765]
44. Sheldrick GM. A short history of SHELX. Acta Crystallogr. A. 2008; 64:112–122. [PubMed: 18156677]
45. Collaborative Computational Project, Number 4. The CCP4 suite: programs for protein crystallography. Acta Crystallogr. D Biol. Crystallogr. 1994; 50:760–763. [PubMed: 15299374]
46. Brunger AT, et al. Crystallography NMR system: a new software suite for macromolecular structure determination. Acta Crystallogr. D Biol. Crystallogr. 1998; 54:905–921. [PubMed: 9757107]
47. Brunger AT. Version 1.2 of the crystallography and NMR system. Nat. Protoc. 2007; 2:2728–2733. [PubMed: 18007608]
48. Storoni LC, McCoy AJ, Read RJ. Likelihood-enhanced fast rotation functions. Acta Crystallogr. D Biol. Crystallogr. 2004; 60:432–438. [PubMed: 14993666]
49. Yousef MR, Grundy FJ, Henkin TM. tRNA requirements for *glyQS* antitermination: a new twist on tRNA. RNA. 2003; 9:1148–1156. [PubMed: 12923262]
50. McDaniel BA, Grundy FJ, Henkin TM. A tertiary structural element in S box leader RNAs is required for *S*-adenosylmethionine-directed transcription termination. Mol. Microbiol. 2005; 57:1008–1021. [PubMed: 16091040]
51. Grundy FJ, Moir TR, Haldeman MT, Henkin TM. Sequence requirements for terminators and antiterminators in the T box transcription antitermination system: disparity between conservation and functional requirements. Nucleic Acids Res. 2002; 30:1646–1655. [PubMed: 11917026]
52. Grundy FJ, Henkin TM. tRNA as a positive regulator of transcription antitermination in *B. subtilis*. Cell. 1993; 74:475–482. [PubMed: 8348614]
53. Anagnostopoulos C, Spizizen J. Requirements for transformation in *Bacillus subtilis*. J. Bacteriol. 1961; 81:741–746. [PubMed: 16561900]
54. Miller, JH. Experiments in Molecular Genetics. Cold Spring Harbor, NY: Cold Spring Harbor Laboratory Press; 1972.

NIH-PA Author Manuscript
NIH-PA Author Manuscript
NIH-PA Author Manuscript

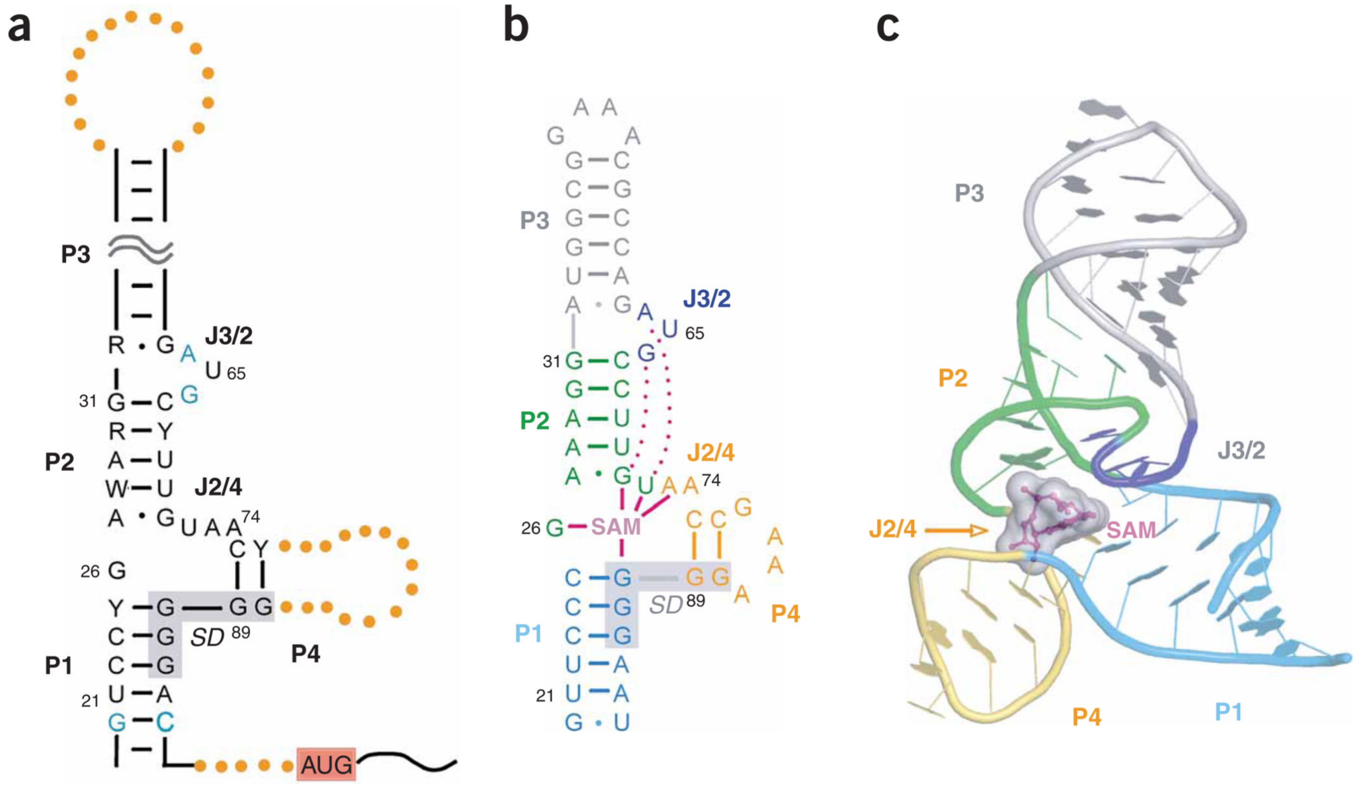

Figure 1.

Structure of the S_{MK} box riboswitch. (**a**) Secondary structure of the S_{MK} box riboswitch based on phylogenetic analysis[24]. Black capital letters, residues that are 100% conserved; blue, 50–85% conserved; R, G or A; W, A or U; Y, C or U; thick dotted lines, hypervariable loops; solid ladders, conserved secondary structure; gray and pink shaded areas, SD sequence and AUG start codon, respectively. (**b**) Secondary structure of the $S_{MK}6$ riboswitch RNA based on the crystal structure. Helices P1 through P4 are colored in cyan, green, silver and yellow, respectively. Gray shading, SD sequence; solid magenta lines, direct contacts between the RNA and the SAM molecule; dashed magenta lines, tertiary interactions between J3/2 and P2 and J2/4. Numbering is consistent with previous studies[24,35]. (**c**) Cartoon representation of the crystal structure of the S_{MK} riboswitch. SAM is shown in overlapping CPK and surface representations in magenta and silver, respectively. The coloring scheme for the RNA is consistent with **b**.

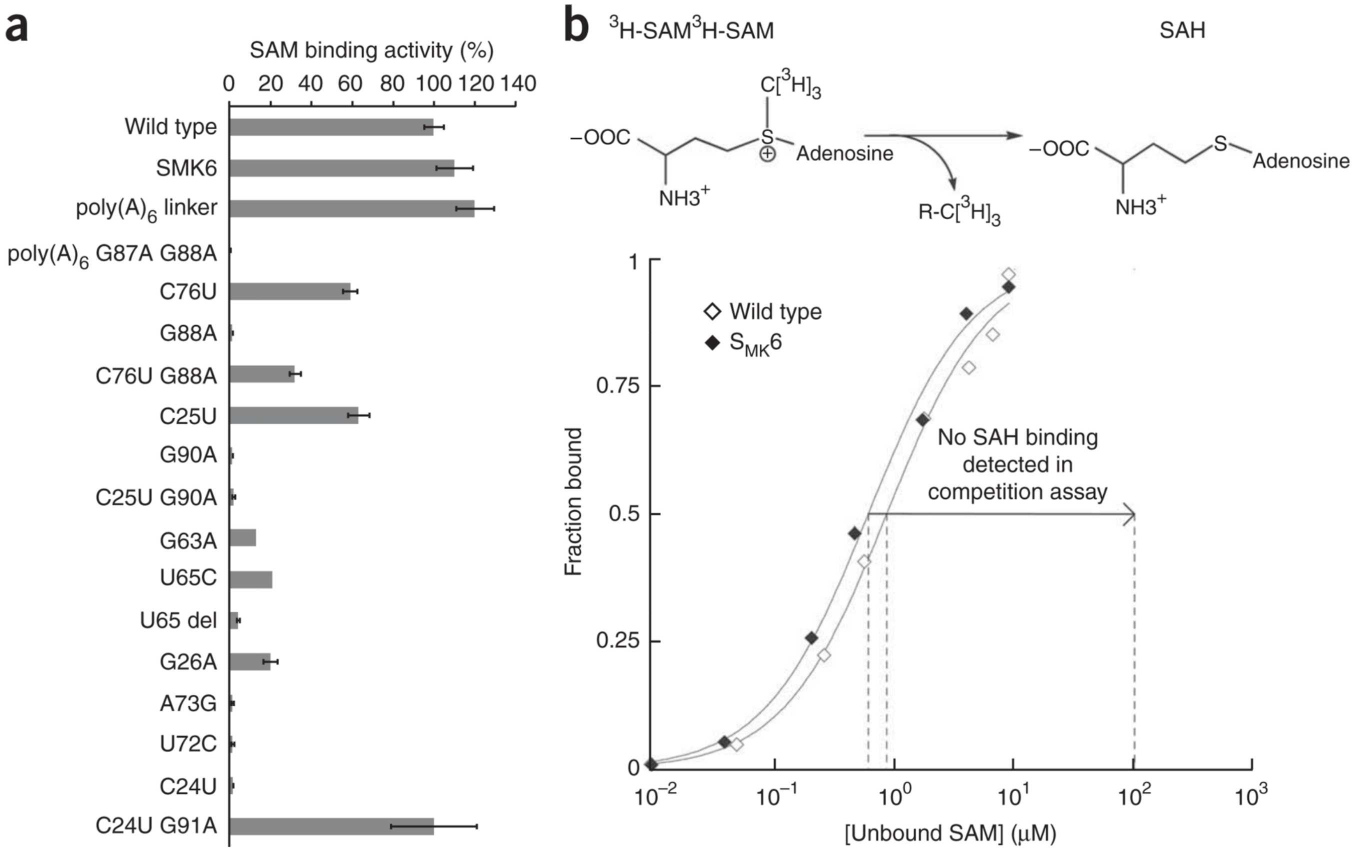

Figure 2.

Effects of S_{MK} box riboswitch mutagenesis on SAM binding and apparent SAM binding constant (K_d) determination. (**a**) Effects of mutation (with s.d.) on SAM binding by size-exclusion filtration assay, as described[24,35]. (**b**) SAM and SAH K_d determination by competition binding assay. Binding curves are shown for the full-length *E. faecalis metK* RNA (open diamonds, K_d = 0.85 μM) and the S_{MK}6 crystallization construct (filled diamonds, K_d = 0.57 μM). Unlabeled SAH showed no competition at a > 100-fold excess of SAH over SAM.

NIH-PA Author Manuscript
NIH-PA Author Manuscript
NIH-PA Author Manuscript

NIH-PA Author Manuscript
NIH-PA Author Manuscript
NIH-PA Author Manuscript

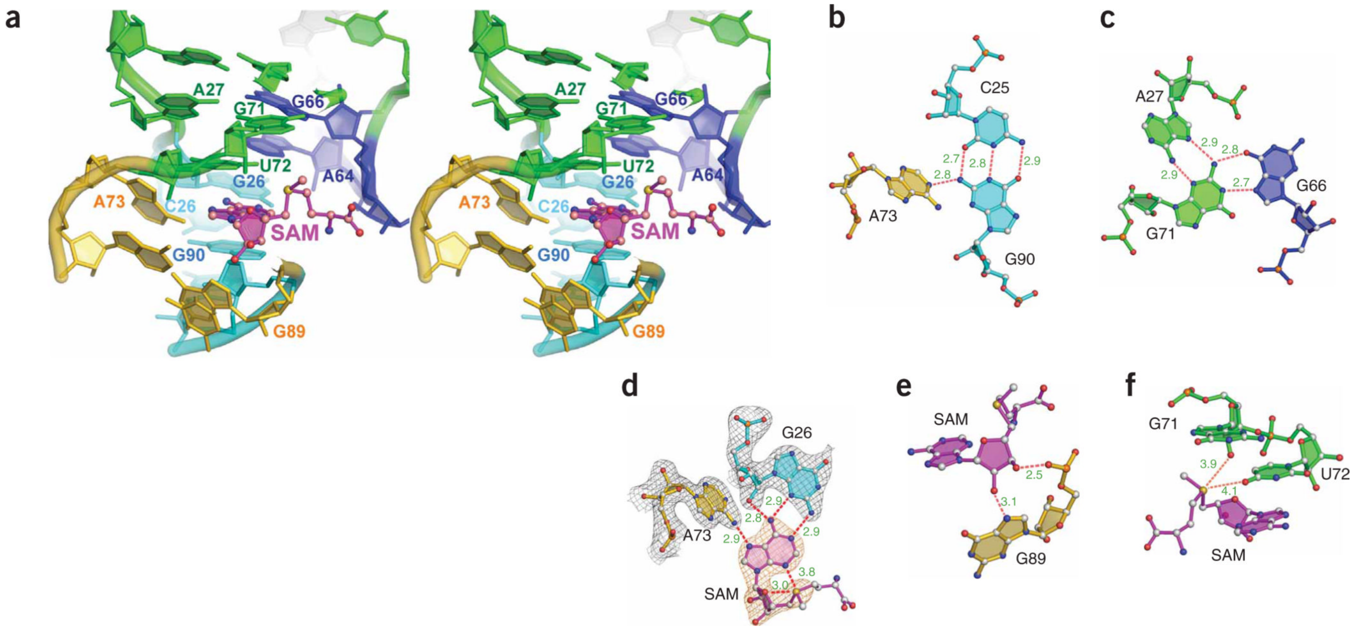

Figure 3.

SAM binding pocket and important interactions. The labeling and base coloring scheme are consistent with that in Figure 1. (**a**) Stereo view of the SAM binding site in the S_{MK} box riboswitch. The adenosine moiety of SAM is shown to base-stack between U72 and G90. (**b**) The A73•G90-C35 base triple paves the 'floor' of the SAM binding pocket. The C-G base pair is co-planar, whereas A73 contacts from the minor groove of G90 at a 45° tilted angle, which orients N6 of A73 for SAM recognition one base plane above. (**c**) The A27•G71•G66 base triple defines the 'ceiling' of the binding pocket, where the sheared A27•G71 base pair in P2 is contacted at the major groove side by G66 of the J3/2 bulge. (**d**) Recognition of the adenosine base of SAM overlapped with the 2.2-Å experimental electron-density contoured at 1.5 σ. Atoms beyond sulfur in SAM do not have corresponding electron density, indicating disorder. The adenine of SAM is extensively recognized through hydrogen-bond interactions from A73 and G26. SAM has two intramolecular electrostatic interactions from the sulfonium ion to the O4′ and N3 of SAM. Grey mesh, RNA density; orange mesh, SAM density. (**e**) The 3′-hydroxyl group of the ribose of SAM is recognized by a hydrogen bond to the phosphoryl oxygen of G89, whereas the 2′-OH makes a rare π–hydrogen bond interaction with the N7 of G89. (**f**) The positively charged sulfonium ion of SAM makes favorable electrostatic interactions with O4 of U72 and the 2′-hydroxyl group of G71. Distances are given in angstroms. Carbon, oxygen, nitrogen, sulfur and phosphorus atoms are colored gray, red, blue, yellow and orange, respectively.

NIH-PA Author Manuscript

NIH-PA Author Manuscript

NIH-PA Author Manuscript

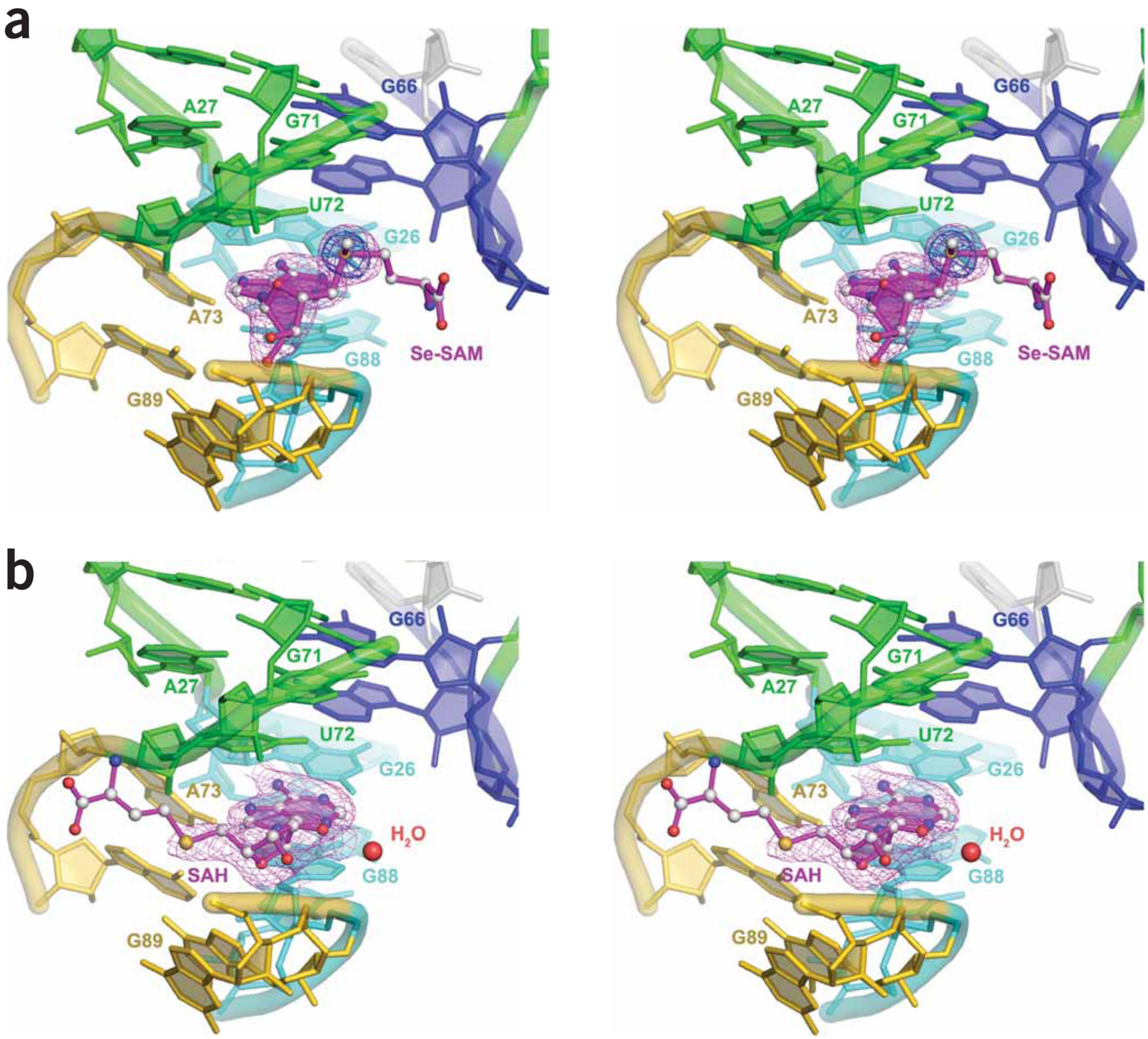

Figure 4.

Binding of Se-SAM and SAH to the S_{MK} box riboswitch. (**a**) Stereo view of the binding pocket in the S_{MK} box riboswitch in complex with Se-SAM. The location of the selenium atom is confirmed by the strong anomalous-difference density shown in blue contoured at 8 σ. The rest of the binding pocket in the Se-SAM–bound S_{MK} structure is almost identical to that in the SAM-bound structure. Magenta mesh signifies the simulated composite omit electron-density map of Se-SAM contoured at 1.5 σ. (**b**) Stereo view of the SAH-bound S_{MK} structure from a direction similar to that shown in **a**. The simulated annealing omit map contoured at 0.8 σ level clearly shows that the ribose and sulfide moieties rotate 180° to exit the RNA from the linker helix side.

NIH-PA Author Manuscript
NIH-PA Author Manuscript
NIH-PA Author Manuscript

Table 1

Expression of *E. faecalis metK-lacZ* fusions

	−Met	+Met	Ratio[b]
Wild type	120 ± 19[a]	24 ± 5.5	5.0
C24G	110 ± 14	95 ± 6.1	1.2
C24U	310 ± 0.71	200 ± 22	1.6
C24U+G91A	23 ± 2.9	15 ± 2.9	1.5
U22G	220 ± 27	160 ± 13	1.4
A93C	77 ± 8.7	42 ± 1.0	1.8
U22G+A93C	11 ± 3.7	2.5 ± 0.72	4.4
C25U	225 ± 25	80 ± 5.0	2.8
C25U+G90A	78 ± 19	82 ± 16	0.95

[a]β-Galactosidase activities are expressed in Miller units[54].

[b]Ratio of expression during growth in the absence of methionine to expression during growth in the presence of methionine.

NIH-PA Author Manuscript
NIH-PA Author Manuscript
NIH-PA Author Manuscript

Table 2

Crystallographic statistics

	S_{MK} native bound to SAM #1	S_{MK} native bound to SAM #2	S_{MK} Ir derivative	S_{MK} bound to Se-SAM	S_{MK} bound to SAH
Data collection					
Space group	$I4_122$	$P4_12_12$	$P4_12_12$	$I4_122$	$I4_122$
Cell dimensions					
a, *b*, *c* (Å)	97.806, 97.806, 87.138	98.131, 98.131, 86.262	98.180, 98.180, 86.790	96.776, 96.776, 86.765	98.148, 98.148, 86.393
Resolution (Å)	20 (2.2)	20 (2.6)	20 (3.3)	20 (2.7)	20 (2.9)
R_{sym}	7.1 (30.3)	11.3 (40.1)	13.3 (42.2)	7.6 (28.4)	7.9 (24.6)
$I / \sigma I$	29.4 (1.2)	12.3 (2.59)	13.2 (5.8)	15.5 (1.7)	80.8 (11.4)
Completeness (%)	95.1 (75.4)	90.4 (85.0)	100 (100)	93.7 (74.0)	100 (100)
Redundancy	9.4 (2.3)	6.3 (4.8)	13.7 (13.6)	3.9 (2.8)	9.3 (8.0)
Refinement					
Resolution (Å)	2.2			2.7	2.9
No. reflections	9,147			4,980	4,694
R_{work} / R_{free}	22.1 / 22.7			22.7 / 25.5	22.2 / 25.9
No. atoms					
RNA	1,155			1,155	1,155
Ligand/ion	42			43	31
Water	69			11	5
B-factors	53			57	56
RNA	50			57	57
Ligand/ion	55			62	49
Water	53			45	44
R.m.s. deviations					
Bond lengths (Å)	0.008			0.005	0.006
Bond angles (°)	1.61			1.29	1.43

*Values in parentheses are for highest-resolution shell.